PERGAMON

International Journal of Heat and Mass Transfer 44 (2001) 155–167

International Journal of HEAT and MASS TRANSFER

www.elsevier.com/locate/ijhmt

The Karhunen–Loève Galerkin method for the inverse natural convection problems

H.M. Park*, W.S. Jung

Department of Chemical Engineering, Sogang University, Shinsoo-Dong, Mapo-Gu, Seoul, South Korea

Received 2 August 1999; received in revised form 14 February 2000

Abstract

The Karhunen–Loève Galerkin method, which is a type of Galerkin method that employs the empirical eigenfunctions of the Karhunen–Loève decomposition as basis functions, is shown to solve inverse natural convection problems efficiently. The specific problem investigated is the inverse natural convection problem of determining the time-varying strength of a heat source from temperature measurement in the domain. The Karhunen–Loève Galerkin procedure can reduce the Boussinesq equation to a set of minimal number of ordinary differential equations by limiting the solution space to the smallest linear subspace that is sufficient to describe the observed phenomena. The performance of the present technique of inverse analysis using the Karhunen–Loève Galerkin procedure is assessed in comparison with the traditional technique of employing the Boussinesq equation, and is found to be very accurate as well as efficient.

1. Introduction

Contrary to the direct problem which consists of computing the consequences of given causes, the inverse problem is associated with the reversal of the cause–effect sequence and consists of finding the unknown causes of known consequences. In many situations, the direct measurement of the cause is impossible or not practical and one is forced to estimate the cause from the observation of the effect. There are many such situations in heat transfer. For example, the temperature of very hot surface is not easily measured directly with sensors. Usually sensors are placed beneath the surface and the temperature of hot surface is estimated by inverse analysis.

The solution of these inverse problems is not straightforward due to their ill-posedness; small perturbations in the observed functions may result into large changes in the corresponding solutions. The ill-posedness requires special numerical techniques to stabilize the results of calculations. Commonly adopted techniques for the solution of inverse heat conduction problems (IHCP) are the least-square methods modified by the addition of regularization terms that impose additional restrictions on admissible solutions and the conjugate gradient method where the regularization is inherently built in the iterative procedure [1]. These inverse algorithms are iterative and therefore require repeated computation of the governing equations before obtaining estimations. Contrary to inverse heat conduction problems, inverse convection problems have not been addressed frequently, partly due to their mathematical complexity in comparison with the inverse heat conduction. Convective heat transfer is governed by a set of nonlinear partial differential

* Corresponding author. Tel.: +82-2-705-8482.
E-mail address: hmpark@ccs.sogang.ac.kr (H.M. Park).

0017-9310/01/$ - see front matter
PII: S0017-9310(00)00092-2

Nomenclature

a_i	the ith velocity spectral coefficient
b_i	the ith temperature spectral coefficient
$d(t)$	conjugate direction of the regular conjugate gradient method
$D(t)$	conjugate direction of the modified conjugate gradient method
$G(t)$	time-varying function of the dimensionless strength of heat source
H_{jl}	matrix defined in Eq. (21)
J	performance function
L_{jl}	matrix defined in Eq. (25)
MO	number of measurement points
M_j	vector defined in Eq. (19)
N_j	vector defined in Eq. (23)
NM	number of velocity eigenfunctions employed
NT	number of temperature eigenfunctions employed
P	pressure
Pr	Prandtl number
P_j	vector defined in Eq. (26)
Q_{jlm}	matrix defined in Eq. (20)
R	Rayleigh number
R_{jlm}	matrix defined in Eq. (24)
S_{jl}	matrix defined in Eq. (22)
t	time
t_f	terminal time
T	dimensionless temperature field
v	dimensionless velocity field

Greek symbols

γ	coefficient defined in Eq. (38)
$\delta(x)$	Dirac delta function
$\delta_n(x)$	function defined in Eq. (4)
δa_i	variation of the spectral coefficient a_i
δb_i	variation of the spectral coefficient b_i
δG	variation of $G(t)$
δJ	variation of the performance function
∇J	gradient of the performance function
η	adjoint temperature field
λ	adjoint velocity field
ρ	optimal step length defined in Eq. (40)
ϕ_i	the ith velocity eigenfunction
φ_i	the ith temperature eigenfunction
Ω	system domain

Superscript

†	measured variable

Subscript

m	measurement point

equations such as, the continuity equation, the Navier–Stokes equation and the energy equation. Since the inverse analysis requires repeated computation of governing equations, it is never trivial to solve inverse convection problems, and very few papers devoted to inverse convection have been published so far. Moutsoglou [2] and Huang and Özisik [3] considered inverse convection problems where the governing equations were greatly simplified to facilitate the analysis and numerical computations. More recently, Prud'homme and Nguyen [4] considered an inverse natural convection problem employing a conjugate gradient method. They adopted the stream function–vorticity formulation to describe the flow field and use the adjoint variable method to determine the conjugate direction. Park and Chung [5] considered an inverse natural convection problem of determining the unknown strength of a time-varying heat source in a cavity from the temperature measurement within the flow. The governing equation of the natural convection, the Boussinesq equation, is employed without any simplification to determine the velocity and temperature fields. The inverse problem is posed as an optimization problem which is solved by a conjugate gradient method, employing the adjoint equation to obtain the descent direction. The difficulty of obtaining the correct conjugate direction at the end point is overcome by employing the modified conjugate gradient method [3,6]. Since the governing equation is not simplified in Park and Chung [5], it can be applied to many different inverse convection problems to yield rigorous results.

Perhaps one of the most important obstacles to the rigorous analysis of the inverse natural convection problems is the tremendous requirement of computer time, since the algorithms of inverse analysis are basically iterative. The repeated numerical solution of the multidimensional Boussinesq equation is quite demanding computationally. Therefore, one of the most important prerequisites for the successful implementation of a rigorous inverse analysis of convection problems is the development of a reliable reduced order model, that is not mathematically complicated but still predicts the system behaviors with accuracy. An appropriate technique for this purpose is the Karhunen–Loève Galerkin procedure [7,8], which is a Galerkin method employing the empirical eigenfunctions of the Karhunen–Loève decomposition as basis functions. With the empirical eigenfunctions, one can a

priori limit the function space considered to the smallest linear subspace that is sufficient to describe the observed phenomena, and thus convert the governing equations to a model with a minimum degree of freedom, resulting in a drastic reduction of computation time without loss of accuracy. Park and Cho [7] has demonstrated that the dynamics of a flow reactor, governed by a convection–diffusion equation with a complicated flow field, can be described faithfully by a small number of ordinary differential equations with the help of the Karhunen–Loève Galerkin procedure. In Park et al. [8], the Karhunen–Loève Galerkin procedure has been successfully applied to the inverse heat conduction problem.

In the present investigation, we apply the Karhunen–Loève Galerkin procedure to the solution of an inverse natural convection problem of estimating the time-varying strength of a heat source. In our previous work [5], this problem was solved by means of a traditional method employing the Boussinesq equation. It shall be shown that the Karhunen–Loève Galerkin procedure reduces the Boussinesq equation to a small number of nonlinear ordinary differential equations, which can be employed in the inverse analysis of natural convection efficiently with sufficient accuracy. The details of the Karhunen–Loève Galerkin procedure are well documented in our previous works [7,8], and references therein. In the following sections, we recapitulate the system description and governing equations with relevant boundary conditions. The procedure of construction of the low-dimensional model and its performance shall also be addressed in detail. Finally, the inverse natural convection problem of estimating the strength of a heat source from the temperature measurements in the domain shall be solved by employing the low-dimensional model, and the efficiency and accuracy of the Karhunen–Loève Galerkin procedure for the solution of inverse natural convection problems shall be addressed.

2. The system and governing equations

We consider a two-dimensional square domain with a time-varying heat source $G(t)$ located at $(x^\dagger, y^\dagger)$. The inverse problem at hand is the estimation of the unknown function $G(t)$ from the temperature readings of a thermocouple located inside the domain. Employing the dimensionless variables introduced in our previous work [5], the set of governing equations may be written as,

$$\nabla \cdot v = 0 \tag{1}$$

$$\frac{\partial v}{\partial t} + v \cdot \nabla v = -\nabla P + Pr\nabla^2 v + R\,Pr\,Tj \tag{2}$$

$$\frac{\partial T}{\partial t} + v \cdot \nabla T = \nabla^2 T + G(t)\delta_n\left(x - x^\dagger\right)\delta_n\left(y - y^\dagger\right) \tag{3}$$

where Pr is the Prandtl number and Ra is the Rayleigh number. The function $\delta_n(x)$, which approximates the point source in the domain, is defined by:

$$\delta_n\left(x - x^\dagger\right) = \frac{n}{2\cosh^2\left(n\left(x - x^\dagger\right)\right)} \tag{4}$$

and becomes the Dirac delta function as n approaches infinity. As earlier [5], we take $n = 20$ with the dimensionless value of $(x^\dagger, y^\dagger) = (0.75, -0.75)$. The relevant initial and boundary conditions are

$$t = 0, \quad v = 0, \quad T = 0 \tag{5}$$

$$x = \pm 1, \quad v = 0, \quad \frac{\partial T}{\partial x} = 0 \tag{6}$$

$$y = \pm 1, \quad v = 0, \quad T = 0 \tag{7}$$

The set of Eqs. (1)–(3) is solved by using the Chebyshev pseudospectral method [5,9] employing (40×20) grids, which is found to be sufficient to resolve the temperature and velocity fields. The range of Rayleigh number considered in this investigation is between 4000 and 20,000.

Fig. 1 depicts the system and boundary conditions. In the same figure, a typical flow pattern and isotherms are plotted together with the shape of the heat source whose strength is indicated by darkness. The nonuniform grid system employed in the Chebyshev pseudospectral method is also superimposed in the same figure.

3. The low-dimensional dynamic model

In this section, we reduce the set of governing Eqs. (1)–(3) with the relevant boundary conditions (5)–(7) to a small number of ordinary differential equations by means of the Karhunen–Loève Galerkin procedure. Before applying the Karhunen–Loève Galerkin procedure to reduce the degree of freedom of the system, we need a set of empirical eigenfunctions which span the solution space of the system for the ranges of parameters of interest. According to the Schmidt–Hilbert theory [7,10], the empirical eigenfunctions $\phi_i(x)$ can be expressed linearly in terms of N snapshots:

$$\phi_i(x) = \sum_{j=1}^{N} \alpha_{(j)}^i v_j(x) \tag{8}$$

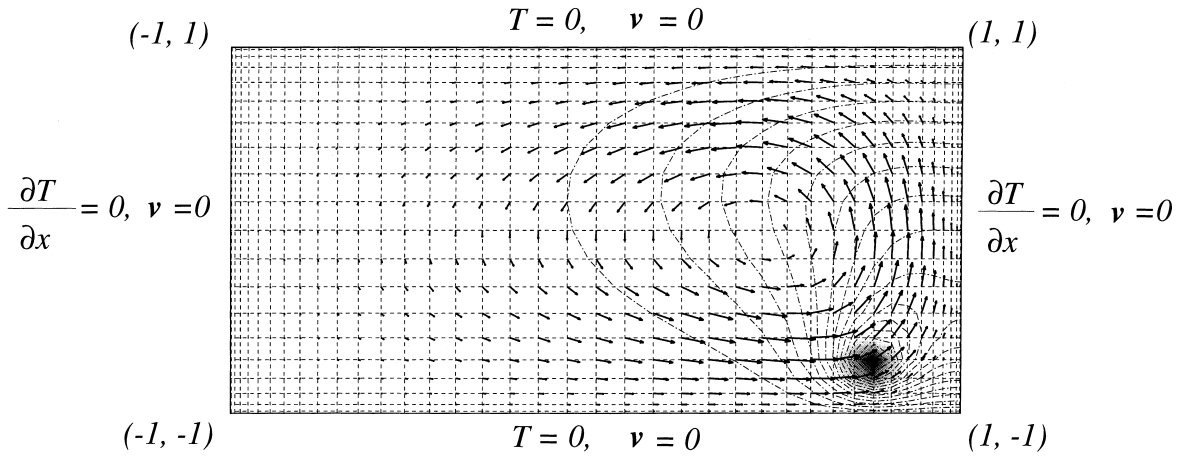

Fig. 1. The system and relevant boundary conditions.

where $v_j(x)$ is the jth snapshot. Therefore, these useful eigenfunctions can be obtained only from an ensemble of snapshots which are representative of the system characteristics [7,8]. An ensemble of snapshots characterizing the system dynamics is obtained in the following way. While imposing a step change on $G(t)$ from 0.0 to 5, we solve the set of Eqs. (1)–(3) and record the transient velocity and temperature fields at a certain time interval until the first steady state is reached. In this way, we obtain 250 velocity and 250 temperature snapshots. Using the first steady state as the initial condition, we solve the governing equations again with $G(t) = 15$ until the second steady state is attained. During this period we obtain another 250 velocity and 250 temperature snapshots. Finally, additional 250 velocity and 250 temperature snapshots are obtained by solving the governing equations with $G(t) = 30$ using the second steady state as the initial condition until the steady state is reached. In this way, we obtain sets of 750 velocity and 750 temperature snapshots. When the Karhunen–Loève decomposition technique [7,8] is applied to the set of velocity and temperature snapshots, respectively, we get velocity and temperature eigenfunctions in the order of their importance in characterizing the system. These empirical eigenfunctions are mutually orthogonal [7,8]. Fig. 2(a)–(f) show the first, second, third, 23rd, 24th and 25th velocity eigenfunctions with the corresponding normalized eigenvalues, $\lambda_1 = 0.9832$, $\lambda_2 = 1.3204 \times 10^{-2}$, $\lambda_3 = 1.7081 \times 10^{-3}$, $\lambda_{23} = 4.8205 \times 10^{-8}$, $\lambda_{24} = 4.6736 \times 10^{-8}$, $\lambda_{25} = 4.5465 \times 10^{-8}$, respectively. Similarly, Fig. 3(a)–(f) show the first, second, third, 25th, 26th and 27th temperature eigenfunctions with the corresponding normalized eigenvalues, $\lambda_1 = 0.9712$, $\lambda_2 = 2.2897 \times 10^{-2}$, $\lambda_3 = 3.0324 \times 10^{-3}$, $\lambda_{25} = 3.2397 \times 10^{-8}$, $\lambda_{26} = 3.1183 \times 10^{-8}$, $\lambda_{27} = 3.0759 \times 10^{-8}$, respectively. As usual, the empirical eigenfunctions with large eigenvalues represent the large scale structures of the velocity and temperature fields, while the empirical eigenfunctions with small eigenvalues represent small scale structures of the corresponding fields.

Using these empirical eigenfunctions, we can reduce the Boussinesq equation to a set of small number of ordinary differential equations. We assume:

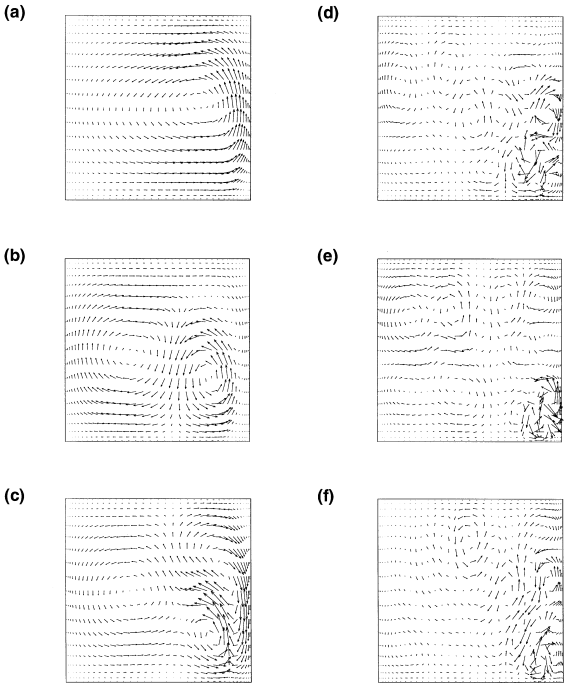

Fig. 2. Velocity eigenfunctions. (a) The first; (b) the second; (c) the third; (d) the 23rd; (e) the 24th; (f) the 25th.

$$v = \sum_{n=1}^{NM} a_n(t)\phi_{(n)}(x, y) \tag{9}$$

$$T = \sum_{n=1}^{NT} b_n(t)\varphi_{(n)}(x, y) \tag{10}$$

where $\phi_{(n)}$ is the nth velocity eigenfunction, $\varphi_{(n)}$ is the nth temperature eigenfunction, a_n is the nth velocity spectral coefficient, b_n is the nth temperature spectral coefficient, NM is the total number of the velocity eigenfunctions employed in the Karhunen–Loève Galerkin procedure, and NT is the total number of the temperature eigenfunctions. When Eqs. (9) and (10) are adopted to represent v and T approximately, the momentum residual R^{M} and the energy residual R^{T} are expressed as:

$$R^{\mathrm{M}} \equiv \frac{\partial v}{\partial t} + v \cdot \nabla v + \nabla P - Pr\,\nabla^2 v - R\,Pr\,Tj \tag{11}$$

$$R^{\mathrm{T}} \equiv \frac{\partial T}{\partial t} + v \cdot \nabla T - \nabla^2 T - G(t)\delta_n\left(x - x^{\dagger}\right)\delta_n\left(y - y^{\dagger}\right) \tag{12}$$

which are usually not equal to zero.

Applying the Galerkin principle which enforces the residual to be orthogonal to each of the basis functions,

$$\int_{\Omega} R^{\mathrm{M}} \cdot \phi_{(j)}\,\mathrm{d}\Omega = 0 \quad (j = 1, 2, \ldots, NM) \tag{13}$$

$$\int_{\Omega} R^{\mathrm{T}} \varphi_{(j)}\,\mathrm{d}\Omega = 0 \quad (j = 1, 2, \ldots, NT) \tag{14}$$

Eqs. (1)–(3) with relevant boundary conditions (5)–(7) are reduced to the following sets of ordinary differential equation

$$M_j \frac{\mathrm{d}a_j}{\mathrm{d}t} + \sum_{l=1}^{NM}\sum_{m=1}^{NM} a_l a_m Q_{jlm} + Pr \sum_{l=1}^{NM} H_{ji} a_l - R\,Pr \sum_{l=1}^{NT} b_l S_{jl} = 0 \tag{15}$$

$$N_j \frac{\mathrm{d}b_j}{\mathrm{d}t} + \sum_{l=1}^{NM}\sum_{m=1}^{NT} a_l b_m R_{jlm} + \sum_{l=1}^{NT} L_{jl} b_l - G(t) P_j = 0 \tag{16}$$

with the initial conditions

$$a_j(t = 0) = \frac{\int_{\Omega} v(x, t = 0) \cdot \phi_{(j)}\,\mathrm{d}\Omega}{M_j} \tag{17}$$

$$b_j(t = 0) = \frac{\int_{\Omega} T(x, t = 0)\varphi_{(j)}\,\mathrm{d}\Omega}{N_j} \tag{18}$$

In the above equations,

$$M_j \equiv \int_{\Omega} \phi_{(j)} \cdot \phi_{(j)}\,\mathrm{d}\Omega \tag{19}$$

$$Q_{jlm} \equiv \int_{\Omega} \phi_{(j)} \cdot \left(\phi_{(l)} \cdot \nabla\phi_{(m)}\right)\mathrm{d}\Omega \tag{20}$$

$$H_{jl} \equiv \int_{\Omega} \left(\nabla\phi_{(j)}\right) : \left(\nabla\phi_{(l)}\right)^{\mathrm{T}}\,\mathrm{d}\Omega \tag{21}$$

$$S_{jl} \equiv \int_{\Omega} \varphi_{(l)}\phi^{v}_{(j)}\,\mathrm{d}\Omega \tag{22}$$

$$N_j \equiv \int_{\Omega} \varphi^2_{(j)}\,\mathrm{d}\Omega \tag{23}$$

$$R_{jlm} \equiv \int_{\Omega} \left(\phi_{(l)} \cdot \nabla\varphi_{(m)}\right)\varphi_{(j)}\,\mathrm{d}\Omega \tag{24}$$

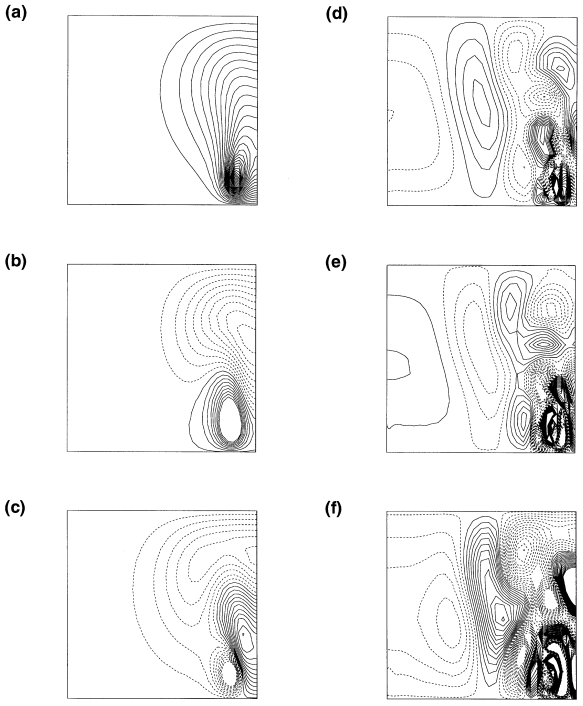

Fig. 3. Temperature eigenfunctions. (a) The first; (b) the second; (c) the third; (d) the 25th; (e) the 26th; (f) the 27th.

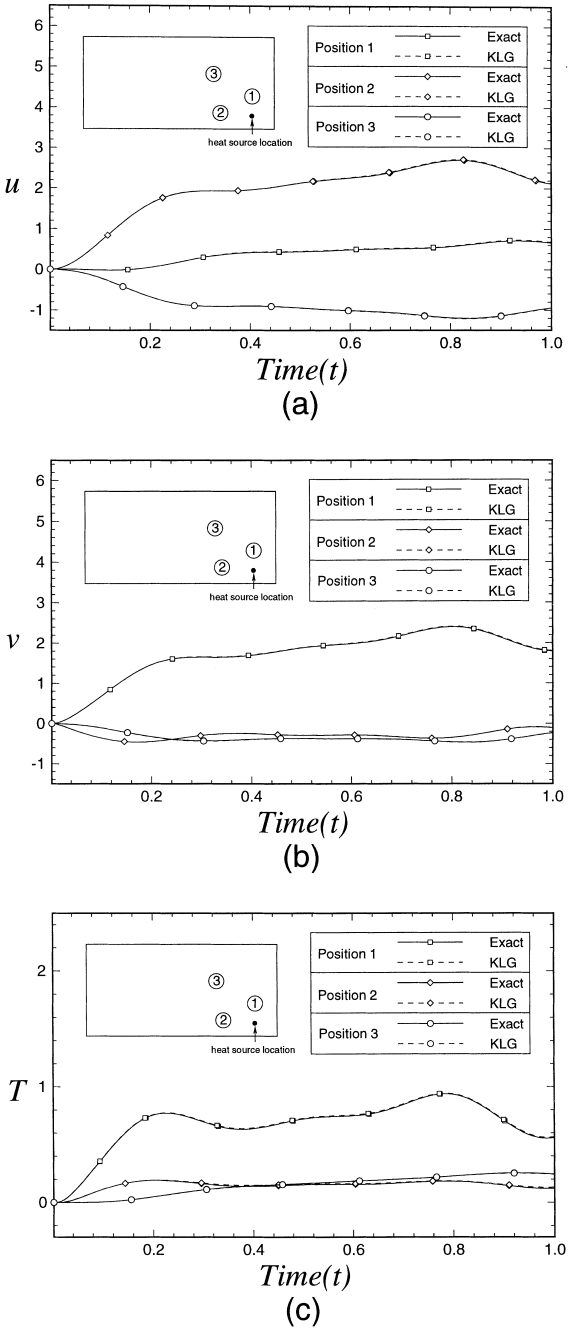

Fig. 4. Comparison of the results of the low-dimensional dynamic model with those of the pseudospectral solution at selected points indicated. (a) x-component of the velocity; (b) y-component of the velocity; (c) temperature.

$$L_{jl} \equiv \int_{\Omega} \nabla\varphi_{(l)} \cdot \nabla\varphi_{(j)} \, \mathrm{d}\Omega \tag{25}$$

$$P_j \equiv \int_{\Omega} \delta_n\left(x - x^{\dagger}\right)\delta_n\left(y - y^{\dagger}\right)\varphi_{(j)} \, \mathrm{d}\Omega \tag{26}$$

where the x- and y-component of the velocity eigenfunctions are denoted by

$$\phi_{(j)} = \left(\phi^{u}_{(j)}, \phi^{v}_{(j)}\right) \tag{27}$$

and Ω is the system domain. The term due to the pressure gradient in Eq. (11) is removed by exploiting the fact that the velocity eigenfunctions $\phi_{(j)}$ are solenoidal and satisfy homogeneous boundary conditions.

The numbers of empirical eigenfunctions employed, NM and NT, are determined by comparing the result of the low-dimensional dynamic model with the numerical solution of the original partial differential equations for a typical heat source function $G(t) = 3 + 0.25\sin(2\pi t) + 1.25\sin(4\pi t) + \sin(6\pi t)$. Usually the error of the low-dimensional model decreases as the number of empirical eigenfunctions employed increases up to the optimal number [7,8]. However, further increase in the number of empirical eigenfunctions beyond the optimal number does not always improve the accuracy because the empirical eigenfunctions with very small eigenvalues are usually contaminated with round-off errors. The optimal numbers of the velocity and temperature eigenfunctions for the set of Eqs. (15) and (16) are found to be $NM = 25$ and $NT = 27$. Employing these number of empirical eigenfunctions, the relative error of the low-dimensional model with respect to the pseudospectral solution of the Boussinesq equation is less than 0.3%. In the sequel, all results of the Karhunen–Loève Galerkin procedure are based on the low-dimensional model constructed using these optimal numbers of eigenfunctions. Fig. 4(a) and (b) show the comparison of velocity components obtained by the low-dimensional dynamic model with those by the pseudospectral solution of the Boussinesq equation at several locations indicated when $G(t)$ varies as given above. The corresponding result for the temperature field is shown in Fig. 4c. It is shown that both, the pseudospectral method and the Karhunen–Loève Galerkin procedure yield almost the same results. These results demonstrate that the set of empirical eigenfunctions employed in the low-dimensional dynamic model spans the admissible solution space of the Boussinesq equation for the specific $G(t)$ given above.

4. Solution of the inverse natural convection problem employing the low-dimensional dynamic model

The temperature field inside the domain, which can be easily measured at various locations, is determined by the heat source function $G(t)$. Therefore, $G(t)$ can be estimated by using the measured values of the temperature field at certain locations. The performance function for the identification of $G(t)$ is expressed by the sum of square residuals between the calculated and observed temperatures as follows:

$$J=\frac{1}{2}\sum_{m=1}^{MO}\int_0^{t_f}\left[T(x_m,y_m,t)-T^{\dagger}(x_m,y_m,t)\right]^2\,\mathrm{d}t \tag{28}$$

where $T(x_m, y_m, t)$ is the calculated temperature, $T^{\dagger}(x_m, y_m, t)$ is the observed temperature at the location (x_m, y_m), and MO is the total number of measurement points. Although only one measurement point is employed in the present work (i.e., $MO=1$) as in our previous investigation [5], summation over the measurement points is kept to make the formula more general.

To minimize the performance function (28), we need the gradient of J, ∇J, which is defined by

$$\delta J(G)\equiv J(G+\delta G)-J(G)\approx\langle\nabla J,\delta G\rangle=\int_0^{t_f}\nabla J\delta G\,\mathrm{d}t \tag{29}$$

where t_f, the final time, is 1.0. The function ∇J can be obtained by introducing the adjoint variables λ_j ($j=1, 2,\ldots,NM$) and η_j ($j=1, 2,\ldots,NT$) such that the performance function can be rewritten as follows:

$$\begin{aligned}J=&\frac{1}{2}\sum_{m=1}^{MO}\int_0^{t_f}\left[\sum_{i=1}^{NT}b_i(t)\varphi_{(i)}(x_m,y_m)-T^{\dagger}(x_m,y_m,t)\right]^2\mathrm{d}t\\&-\sum_{j=1}^{NM}\int_0^{t_f}\lambda_j(t)\left[M_j\frac{\mathrm{d}a_j}{\mathrm{d}t}+\sum_{l=1}^{NM}\sum_{n=1}^{NM}Q_{jln}a_la_n+Pr\sum_{l=1}^{NM}H_{jl}a_l\right.\\&\left.-R\,Pr\sum_{l=1}^{NT}b_lS_{jl}\right]\mathrm{d}t\\&-\sum_{j=1}^{NT}\int_0^{t_f}\eta_j(t)\left[N_j\frac{\mathrm{d}b_j}{\mathrm{d}t}+\sum_{l=1}^{NM}\sum_{n=1}^{NT}a_lb_nR_{jln}+\sum_{l=1}^{NT}L_{jl}b_l\right.\\&\left.-G(t)P_j\right]\mathrm{d}t\end{aligned} \tag{30}$$

After taking a variation of J given by Eq. (30), interchanging the summation indices and setting the resulting equation equal to zero, we find

$$\nabla J=\sum_{j=1}^{NT}\eta_jP_j \tag{31}$$

while the adjoint variables, λ_j and η_j, must satisfy the following equations,

$$\begin{aligned}M_j\frac{\mathrm{d}\lambda_j}{\mathrm{d}t}-&\sum_{l=1}^{NM}\sum_{n=1}^{NM}Q_{ljn}\lambda_la_n-\sum_{l=1}^{NM}\sum_{n=1}^{NM}Q_{nlj}\lambda_na_l\\&-Pr\sum_{l=1}^{NM}H_{lj}\lambda_l-\sum_{l=1}^{NT}\sum_{n=1}^{NT}\eta_lb_nR_{ljn}=0\end{aligned} \tag{32}$$

$$\begin{aligned}N_j\frac{\mathrm{d}\eta_j}{\mathrm{d}t}-&\sum_{n=1}^{NT}\sum_{l=1}^{NM}\eta_na_lR_{nlj}-\sum_{l=1}^{NT}\eta_lL_{lj}+R\,P_r\sum_{l=1}^{NM}S_{lj}\lambda_l\\&+\sum_{m=1}^{MO}\left[\varphi_{(j)}(x_m,y_m)\left\{\sum_{i=1}^{NT}b_i(t)\varphi_{(i)}(x_m,y_m)\right.\right.\\&\left.\left.-T^{\dagger}(x_m,y_m,t)\right\}\right]=0\end{aligned} \tag{33}$$

with the following relevant starting conditions

$$\lambda_j(t=t_f)=0\quad(j=1,2,\ldots,NM) \tag{34}$$

$$\eta_j(t=t_f)=0\quad(j=1,2,\ldots,NT) \tag{35}$$

As in our previous work [5], where the same problem of inverse natural convection has been solved using the original partial differential equation, the Fletcher–Reeves algorithm of conjugate gradient method is used to minimize the performance function. The conjugate direction at the first step is determined by

$$d^0(t)=\nabla J(t)=\sum_{j=1}^{NT}\eta_jP_j \tag{36}$$

Beginning the second iteration step, the conjugate direction is given by

$$d^i(t)=\nabla J^i(t)+\gamma^i d^{i-1}(t) \tag{37}$$

where

$$\gamma^i=\frac{\int_0^{t_f}\left(\nabla J^i(t)\right)^2\mathrm{d}t}{\int_0^{t_f}\left(\nabla J^{i-1}(t)\right)^2\mathrm{d}t} \tag{38}$$

and i is the iteration number. Then the heat source function is updated in the conjugate direction as follows:

$$G^{i+1}=G^i-\rho d^i(t) \tag{39}$$

The optimal step length ρ in the direction $d^i(t)$ is

obtained by minimizing $J(G^i - \rho d^i)$ with respect to ρ:

$$\rho = \frac{\sum_{m=1}^{MO}\int_0^{t_f}\left[\sum_{i=1}^{NT} b_i\varphi_{(i)}(x_m, y_m) - T^{\dagger}(x_m, y_m, t)\right]\left[\sum_{i=1}^{NT}\delta b_i\varphi_{(i)}(x_m, y_m)\right]\mathrm{d}t}{\sum_{m=1}^{MO}\int_0^{t_f}\left[\sum_{i=1}^{NT}\delta b_i\varphi_{(i)}(x_m, y_m)\right]^2\mathrm{d}t} \tag{40}$$

The sensitivity functions δb_i in Eq. (40) are obtained by solving the following sensitivity equations.

$$M_j\frac{\mathrm{d}}{\mathrm{d}t}\delta a_j + \sum_{l=1}^{NM}\sum_{n=1}^{NM} Q_{jln}\delta a_l a_n + \sum_{l=1}^{NM}\sum_{n=1}^{NM} Q_{jln} a_l\delta a_n + Pr\sum_{l=1}^{NM} H_{jl}\delta a_l - R\,Pr\sum_{l=1}^{NT} S_{jl}\delta b_l = 0 \tag{41}$$

$$N_j\frac{\mathrm{d}}{\mathrm{d}t}\delta b_j + \sum_{l=1}^{NM}\sum_{n=1}^{NT}\delta a_l b_n R_{jln} + \sum_{l=1}^{NM}\sum_{n=1}^{NT} a_l\delta b_n R_{jln} + \sum_{l=1}^{NT} L_{jl}\delta b_l = d(t)P_j \tag{42}$$

The relevant initial conditions for the sensitivity equations are

$$\delta a_j(t=0) = 0 \quad (j = 1, 2, \ldots, NM) \tag{43}$$

$$\delta b_j(t=0) = 0 \quad (j = 1, 2, \ldots, NT) \tag{44}$$

The conjugate gradient method as applied to the inverse natural convection problem employing the low-dimensional dynamic model follows the procedure below.

1. Assume the heat source function $G(t)$ and calculate the velocity and temperature fields by solving Eqs. (15) and (16).
2. Solve the adjoint Eqs. (32) and (33).
3. ∇J is determined by Eq. (31).
4. The conjugate direction $d^i(t)$ is given by Eq. (37) with γ^i determined by Eq. (38).
5. Solve the sensitivity Eqs. (41) and (42).
6. The optimal step length in the conjugate direction $d^i(t)$ is given by Eq. (40).
7. The heat source function $G(t)$ is updated according to Eq. (39).
8. Repeat the above procedure until convergence.

5. Modified conjugate gradient approach

As in our previous work [5], the conjugate gradient method employing the adjoint equation does not yield correct estimation of heat source function at the final time $G(t_f)$, which is always equal to the initial guess $G^0(t_f)$. Since the value of η_j is zero at the final time $t = t_f$ (Eq. (35)), ∇J is also zero at $t = t_f$ due to Eq. (31). From Eq. (37), we find that the conjugate direction vanishes at $t = t_f$, and consequently, the heat source function at the final time is left unchanged at $t = t_f$ (cf. Eq. (39)). The difficulty encountered at the final time t_f is alleviated by using the following modified conjugate gradient method [3,5,6]. From Eqs. (29) and (31), the variation of the performance function δJ may be rewritten as:

$$\delta J = \int_0^{t_f}\delta G(t)\left\{\sum_{j=1}^{NT}\eta_j P_j\right\}\mathrm{d}t \tag{45}$$

If Eq. (45) is integrated by parts with respect to t, we find

$$\delta J = -\int_0^{t_f}\frac{\mathrm{d}\delta G}{\mathrm{d}t}\int_{t_f}^{t}\sum_{j=1}^{NT}\eta_j(t')P_j\,\mathrm{d}t'\,\mathrm{d}t \tag{46}$$

Therefore, the derivation of J with respect to $\frac{\mathrm{d}G}{\mathrm{d}t}$ is given by the following expression

$$\nabla J\left(\frac{\mathrm{d}G}{\mathrm{d}t}\right) = -\int_{t_f}^{t}\sum_{j=1}^{NT}\eta_j(t')P_j\,\mathrm{d}t' \tag{47}$$

Then, we take the conjugate direction as follows:

$$d^i(t) = \int_0^t D^i(t')\,\mathrm{d}t' \tag{48}$$

where

$$D^i = \nabla J\left(\frac{\mathrm{d}G}{\mathrm{d}t}\right)^i + \gamma^i D^{i-1} \tag{49}$$

Since $d^i(t_f)$, obtained by Eq. (48), is nonzero, the modified conjugate gradient method yields reasonably accurate estimation of $G(t_f)$, contrary to the previous regular conjugate gradient method. On the other hand, from Eq. (48) it can be seen that $d^i(0) = 0$. Then, for the same reason with the regular conjugate gradient method, the modified conjugate gradient method will

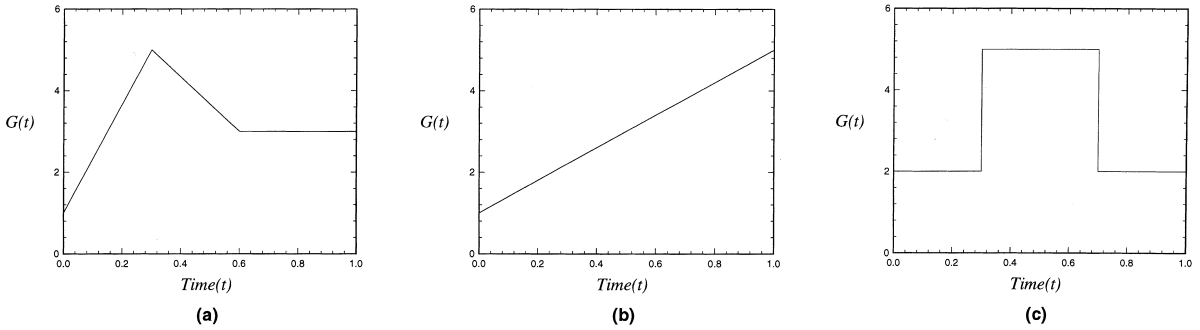

Fig. 5. Various shapes of the heat source functions considered in the present investigation.

not improve the starting value $G(0)$. This dilemma is overcome by combining the regular and modified conjugate gradient methods sequentially. At the first stage, we employ the modified conjugate gradient method for a certain number of iterations until a reasonably good estimation of the end value $G(t_f)$ is attained. Afterwards, the regular conjugate gradient method is adopted using the estimation of the modified conjugate gradient method as the initial approximation, until a converged profile is obtained.

6. Results

We compare the accuracy and efficiency of the Karhunen–Loève Galerkin procedure with those of the traditional method of employing the original partial differential equations for the inverse natural convection problem of estimating the unknown strength of a time-varying heat source $G(t)$ in the domain. To make a fair comparison, we consider the same heat source functions $G(t)$ adopted in Park and Chung [5], where

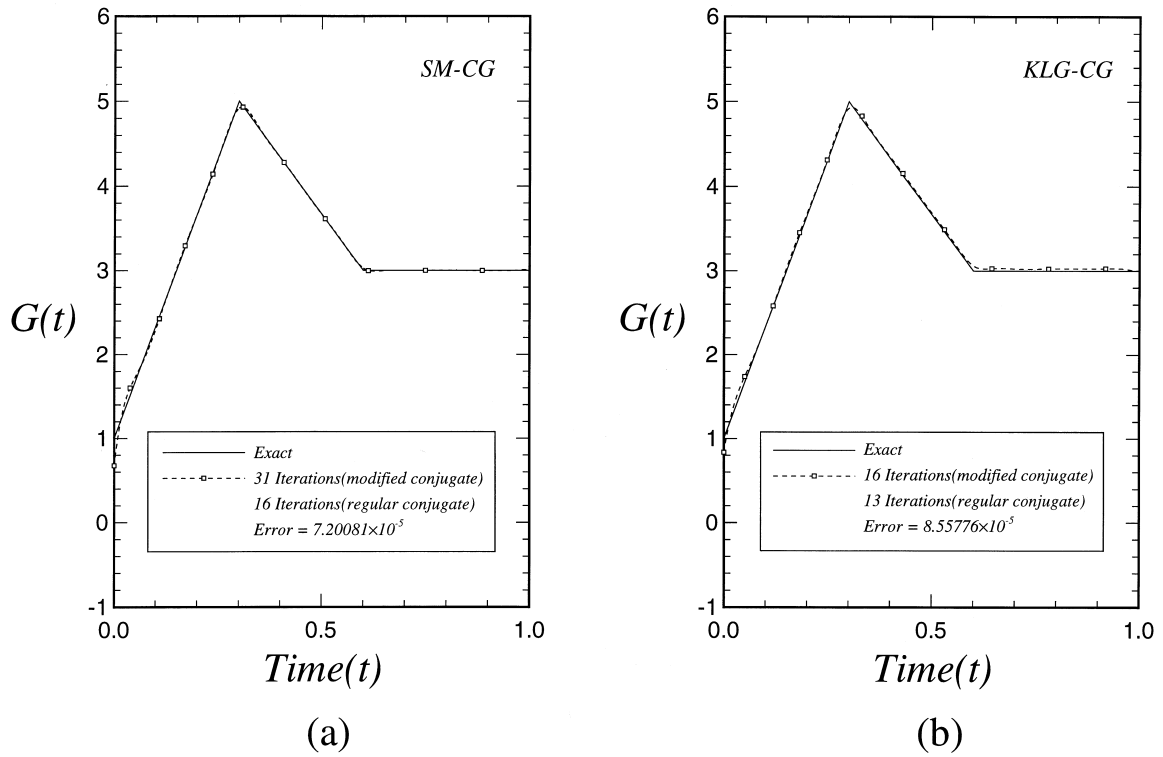

Fig. 6. Estimated heat source function $G(t)$ for the case (a) of Fig. 5 (a) SM-CG; (b) KLG-CG.

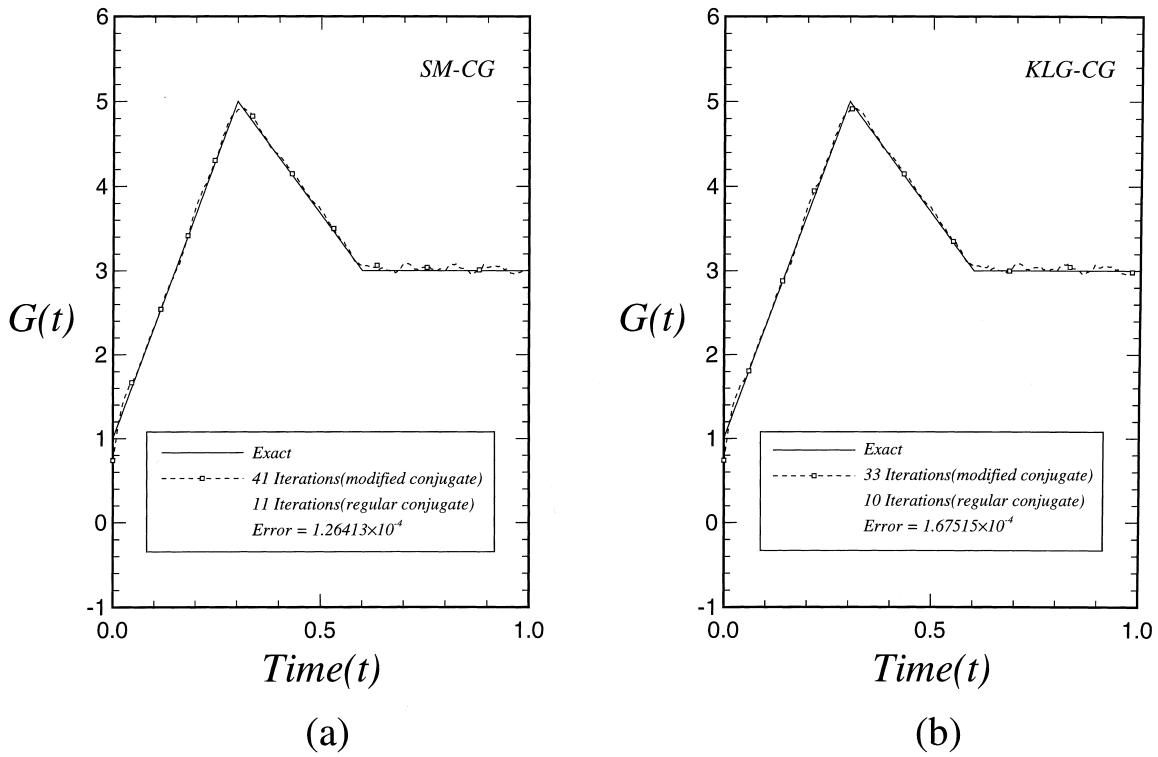

Fig. 7. Estimated heat source function $G(t)$ for the case (a) when the relative measurement error is 3%. (a) SM-CG; (b) KLG-CG.

the same inverse natural convection problem has been solved by using the Boussinesq equation. Fig. 5(a)–(c) depict these heat source functions. The initial approximation of $G(t)$ in the conjugate gradient method is taken to be 0.0 for all numerical experiments reported below. The simulated measurements containing measurement errors are generated by adding Gaussian distributed random errors to the computed exact temperatures. The temperature recordings are assumed to be done continuously by a thermocouple located at the reference position (0.7604, −0.3090). For the estimation of the heat source functions, we employ the combined iteration scheme [5] which involves both the regular and modified conjugate gradient methods. At the first stage, the modified conjugate gradient method is employed for a certain number of iterations until a reasonably good estimation of the end point value $G(t_f)$ is attained. Afterwards, the regular conjugate gradient method is adopted using the estimation of the modified conjugate gradient method as the initial approximation to get the final converged profile. The error of $G(t_f)$ in the modified conjugate gradient method is defined by:

$$E = \sum_{i=1}^{3} \frac{|G^n(t_f) - G^{n-i}(t_f)|}{|G^n(t_f)|} \tag{50}$$

and the iteration of the modified conjugate gradient is stopped when $E < 0.01$.

We first consider an idealized situation in which there are no measurement errors. The detailed algorithm of the conventional method employing the Bous-

Table 1
Comparison of the SM-CG and the KLG-CG; convergence rate, relative estimation error and CPU time

	SM-CG	KLG-CG
Case (a)		
Iteration number (modified)	31	16
Iteration number (regular)	16	13
Relative estimation error	7.20081×10^{-5}	8.55776×10^{-5}
Case (b)		
Iteration number (modified)	41	22
Iteration number (regular)	14	11
Relative estimation error	1.11346×10^{-4}	1.52042×10^{-4}
Case (c)		
Iteration number (modified)	49	46
Iteration number (regular)	26	19
Relative estimation error	4.00022×10^{-3}	4.15266×10^{-3}
CPU time (average)	1.827×10^{-5} (s)	3.996×10^{3} (s)

Table 2
Effect of measurement location on the accuracy of the estimation for the case (a) of Fig. 5

	SM-CG	KLG-CG
Measurement location $\boldsymbol{x}^{\mathrm{I}} = (0.7604, -0.3090)$		
Iteration number (modified)	31	16
Iteration number (regular)	16	13
Relative estimation error	7.20081×10^{-5}	8.55776×10^{-5}
Measurement location $\boldsymbol{x}^{\mathrm{II}} = (0.8092, 0.0)$		
Iteration number (modified)	14	17
Iteration number (regular)	16	11
Relative estimation error	1.71769×10^{-4}	2.54690×10^{-4}
Measurement location $\boldsymbol{x}^{\mathrm{III}} = (0.8526, 0.1564)$		
Iteration number (modified)	17	18
Iteration number (regular)	17	11
Relative estimation error	2.62246×10^{-4}	3.34519×10^{-4}

sinesq equation is well documented in Park and Chung [5]. For brevity, we call the method employing the Boussinesq equation the SM-CG, and that employing the low-dimensional dynamic model the KLG-CG. Fig. 6(a) and (b) shows the estimated profiles for the case (a) of Fig. 5 when using the SM-CG (Fig. 6a) and the KLG-CG (Fig. 6b). It takes 31 modified conjugate gradient iterations and 16 regular conjugate gradient iterations to obtain the converged profile with relative estimation error of 7.20081×10^{-5} when using the SM-CG. On the other hand, it takes 16 modified conjugate gradient iterations and 13 regular conjugate gradient iterations before a converged profile of $G(t)$ with the relative estimation error of 8.55776×10^{-5} is obtained

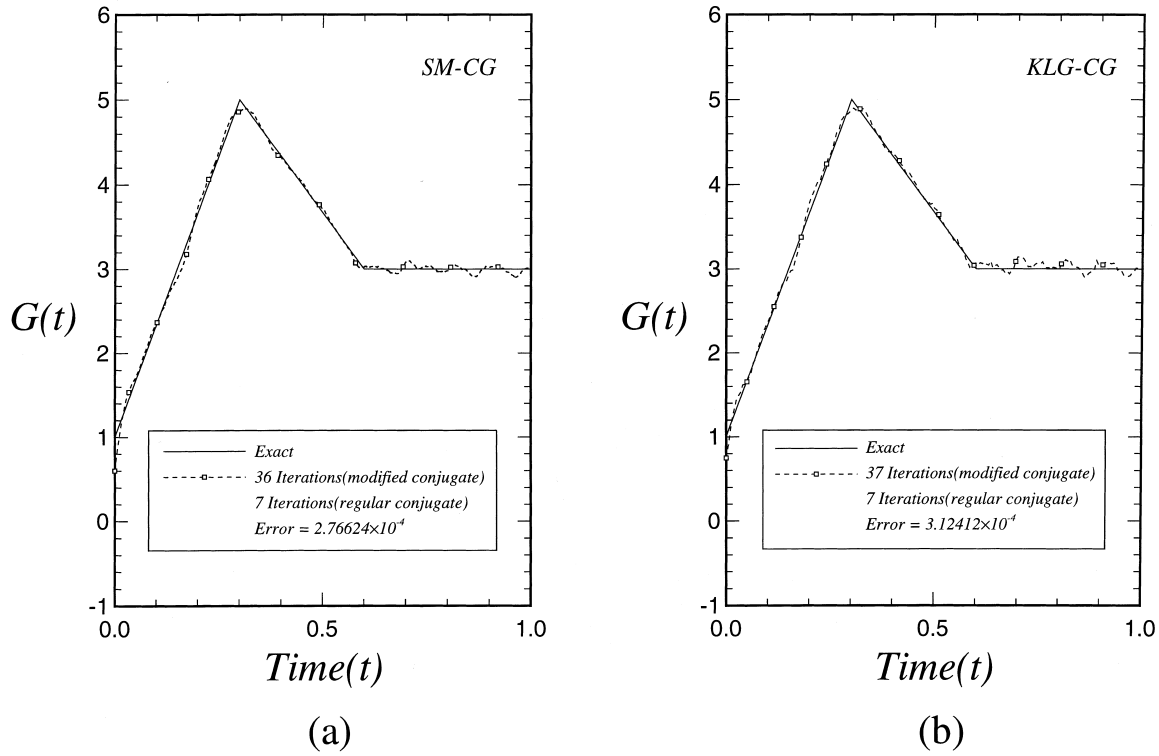

Fig. 8. Estimated $G(t)$ when the relative measurement error is 6%. (a) SM-CG; (b) KLG-CG.

when using the KLG-CG. Table 1 summarizes the comparison of the SM-CG and the KLG-CG for the three cases of Fig. 5 as regards the convergence rate, the relative estimation error and the consumption of CPU time when using the SUN ultrasparc II workstation. It is shown that the convergence rate and the relative estimation error of the KLG-CG are not much different from those of the SM-CG. However, the CPU time consumption of the KLG-CG is about 1/45 of that of the SM-CG on average. This drastic reduction of CPU time with the use of the KLG-CG is not unexpected considering the fact that the degree of freedom of the low-dimensional dynamic model is only 52 while that of the Boussinesq equation, which is equivalent to the grid number employed in the pseudospectral computation multiplied by 4 (u, v, P, T), is about 3200. The CPU time required to obtain the empirical eigenfunctions and construct the low-dimensional dynamic model of the KLG-CG is not significant when compared to the CPU time needed in the conjugate gradient iterations as explained in our previous papers [7,8]. Moreover, once the low-dimensional model is constructed for a given system, it can be employed to estimate various other shapes of heat source function $G(t)$.

Next consideration is the effect of the location of sensor on the accuracy of the estimation. In addition to the previous reference location $\boldsymbol{x}^{\mathrm{I}} = (0.7604, -0.3090)$, we consider two additional locations farther from the heat source than the reference one, i.e., $\boldsymbol{x}^{\mathrm{II}} = (0.8092, 0.0)$, and $\boldsymbol{x}^{\mathrm{III}} = (0.8526, 0.1564)$. The distances between the heat source and the sensor satisfy $|\boldsymbol{x}^{\mathrm{I}} - \boldsymbol{x}^{\mathrm{S}}| < |\boldsymbol{x}^{\mathrm{II}} - \boldsymbol{x}^{\mathrm{S}}| < |\boldsymbol{x}^{\mathrm{III}} - \boldsymbol{x}^{\mathrm{S}}|$, where $\boldsymbol{x}^{\mathrm{S}}$ is the location of the heat source. Table 2 summarizes the results. We find that, both with the SM-CG and the KLG-CG, as the location of the sensor approaches that of heat source, the accuracy improves since the sensitivity of the temperature field with respect to the heat source increases as the distance between the measurement point and the heat source decreases. It is also shown that the accuracy of the estimation obtained by the KLG-CG is comparable to that of the SM-CG.

Figs. 7 and 8 show the effect of measurement error on the accuracy of estimation. When there are measurement errors, we use the following discrepancy principle as the stopping criterion for the conjugate gradient method [3,5,8]. Namely, if the value of the performance function J has been decreased such that

$$J < \epsilon^2 \approx \frac{1}{2}\int_0^{t_{\mathrm{f}}} \sum_{m=1}^{MO} \sigma^2 \, \mathrm{d}t \tag{51}$$

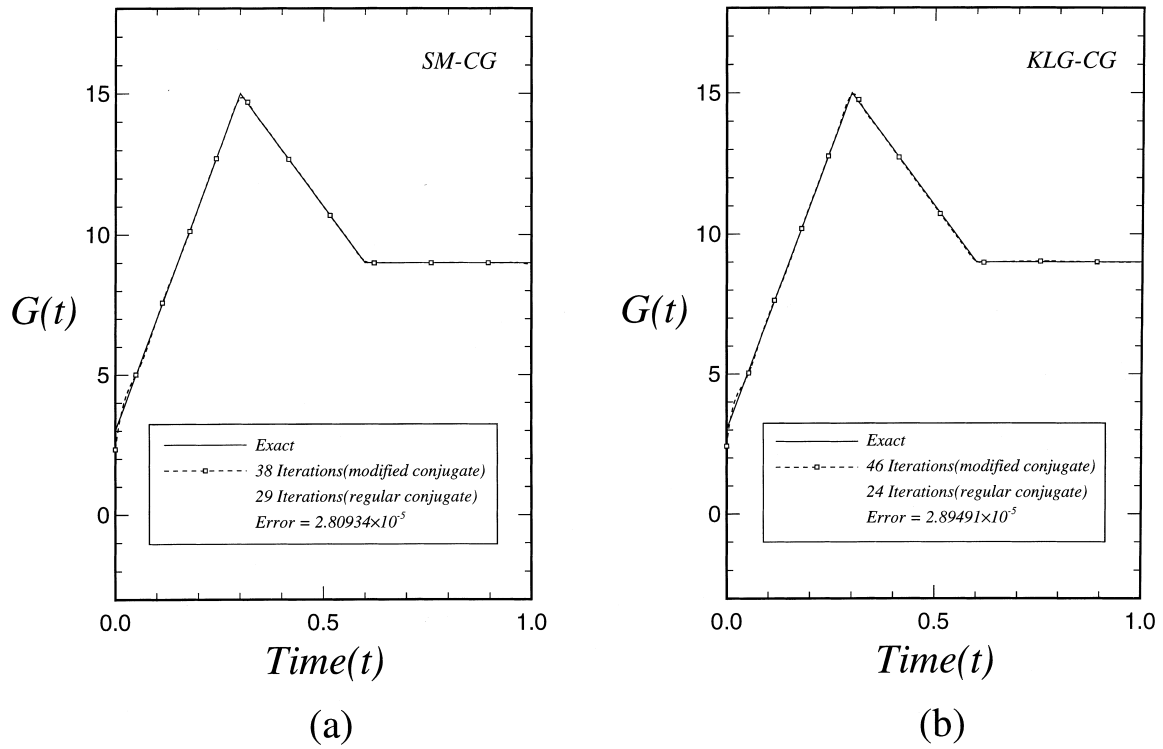

Fig. 9. Estimated heat source function for the case (a) when $G(t)$ is increased by three times. (a) SM-CG; (b) KLG-CG.

we stop the iteration, where σ is the absolute measurement error. Fig. 7a is the estimation obtained by the SM-CG and Fig. 7b is the estimation obtained by the KLC-CG when the relative measurement error is 3%. Fig. 8(a) and (b) show the estimated $G(t)$ obtained by the SM-CG and by the KLG-CG, respectively, when the relative measurement error is 6%. As expected, the accuracy of the estimation deteriorates as the measurement error increases both, with the SM-CG and the KLG-CG. It is also shown than the KLG-CG yields estimations comparable to those of the SM-CG even when there are measurement errors.

Finally, the magnitude of $G(t)$ for the case (a) is increased to three times of the default value given by Fig. 5a. This is equivalent to the increase of Rayleigh number from 4000 to about 12,000. Fig. 9(a) and (b) show the estimated profiles obtained by the SM-CG (Fig. 9a) and by the KLG-CG (Fig. 9b), respectively. Both, the SM-CG and the KLG-CG yield reasonably accurate results. Since the empirical eigenfunctions employed in the low-dimensional dynamic model are constructed in Section 3 such that they span the solution space of the system up to $Ra \approx 24{,}000$ (or $G(t) \approx 30$), the KLG-CG is expected to yield reasonably accurate results up to this range of Rayleigh number.

7. Conclusion

The techniques for the inverse problems are basically iterative and require repeated computation of governing and adjoint equations. Thus, the solution of inverse natural convection problems requires repeated numerical solution of Boussinesq equation and its adjoint equation, and the resulting tremendous consumption of computer time has hindered progresses in the inverse natural convection problems. In the present investigation, we reduced the Boussinesq equation to a small number of ordinary differential equations through the Karhunen–Loève Galerkin procedure, and employed the resulting low-dimensional dynamic model successfully to solve an inverse natural convection problem of estimating the unknown strength of a time-varying heat source from the temperature measurement within the flow. This method of solving the inverse natural convection problem (KLG-CG) has been compared with the traditional method employing the Boussinesq equation [5] (SM-CG) as regards accuracy and efficiency. It is found that the KLG-CG yields estimations as accurate as those of the SM-CG for various shapes of heat source function with various degree of measurement errors at a drastically reduced computer time.

References

[1] Y. Jarney, M.N. Özisik, J.P. Bardon, A general optimization method using adjoint equation for solving multidimensional inverse heat conduction, International Journal of Heat and Mass Transfer 34 (1991) 2911–2919.
[2] A. Moutsoglou, An inverse convection problem, ASME J. Heat Transfer 221 (1989) 37–43.
[3] C.H. Huang, M.N. Özisik, Inverse problem of determining unknown wall heat flux in laminar flow through a parallel duct, Num. Heat Transfer 21 (Part A) (1992) 55–70.
[4] M. Prud'homme, T.H. Nguyen, Whole time-domain approach to the inverse natural convection problem, Num. Heat Transfer 32 (Part A) (1997) 169–186.
[5] H.M. Park, O.Y. Chung, An inverse natural convection problem of estimating the strength of a heat source, International Journal of Heat and Mass Transfer 42 (1999) 4259–4273.
[6] O.M. Alifanov, V.V. Mikhailov, Solution of the nonlinear inverse thermal conductivity problem by the iteration method, J. Engng. Phys 35 (1978) 1501–1506.
[7] H.M. Park, D.H. Cho, Low-dimensional modeling of flow reactors, International Journal of Heat and Mass Transfer 39 (1996) 3311–3323.
[8] H.M. Park, O.Y. Chung, J.H. Lee, On the solution of inverse heat transfer problem using the Karhunen–Loève Galerkin method, International Journal of Heat and Mass Transfer 42 (1999) 127–142.
[9] H.C. Ku, T.D. Taylor, R.S. Hirsh, Pseudospectral methods for solution of the incompressible Navier–Stokes equations, Computer and Fluids 15 (1987) 195–214.
[10] R. Courant, D. Hilbert, Method of Mathematical Physics, vol. I, Wiley–Interscience, New York, 1962.